

Railway slab vs ballasted track: A comparison of track geometry degradation

C. Charoenwong^{a,*}, D.P. Connolly^{a,*}, A. Colaço^b, P. Alves Costa^b, P.K. Woodward^a,
A. Romero^c, P. Galvín^{c,d}

^a Institute for High Speed Rail and Systems Integration, School of Civil Engineering, University of Leeds, UK

^b CONSTRUCT-FEUP, Department of Civil Engineering, Faculty of Engineering, University of Porto, Rua Dr. Roberto Frias s/n, 4200-465 Porto, Portugal

^c Escuela Técnica Superior de Ingeniería, Universidad de Sevilla, Camino de los Descubrimientos s/n, 41092, Sevilla, Spain

^d Laboratory of Engineering for Energy and Environmental Sustainability, Universidad de Sevilla, Camino de los Descubrimientos s/n, 41092 Sevilla, Spain

ARTICLE INFO

Keywords:

Railway track geometry
Track recording car
Railway differential settlement
Concrete slab track
Non-ballasted railway settlement
Railway longitudinal level

ABSTRACT

Concrete slab railway tracks typically have higher initial capital costs yet lower operational costs in comparison to ballasted tracks. One reason for the elevated operational costs on ballasted lines is the need for more frequent maintenance (e.g. tamping to maintain track geometry). Therefore on higher linespeed routes where maintenance windows are limited, concrete slab track is a common choice of trackform. In contrast, on lower linespeed routes it's common to opt for ballasted track structures. However, the speed ranges at which the two different trackforms are most suitable has received limited scientific analysis. Therefore this paper aims to investigate the train-induced differential settlement of ballast and non-ballasted tracks, considering typical modern intercity (200 km/h) and high speed (300 km/h) lines. Vertical railway track geometry is the metric used to analyse maintenance requirements. This is because it defines the longitudinal level of railway tracks and is a common metric used for the scheduling of track maintenance. First a novel numerical model is presented capable of computing track geometry deterioration due to repeated load passages. The model is then validated for both ballast and concrete slab tracks. Finally it is used to study the differential settlement of both track structures at the two train speeds. It is shown that the ballasted track exhibits higher train-induced differential settlement compared to the slab and at higher linespeeds the degradation of track geometry is increasingly pronounced for the ballasted track.

1. Introduction

Railway track structures are typically divided into two main categories: ballasted and non-ballasted. The adoption of one solution over the other is based on a variety of technical and economic requirements, including initial investment and long-term maintenance. For example, France and Spain adopt a predominant ballasted network, while the high-speed network in Germany and China is predominantly non-ballasted. Non-ballasted is a more common choice for lines constructed in the last 20 years [8]. Although the Japanese high speed network now consists of approximately 70% slab track, conventional ballasted track was used for their first high speed line connecting Tokyo and Shin-Osaka in 1964. A comparison between ballasted and non-ballasted high speed lines in Japan shows that the lower maintenance costs associated with slab track can offset the higher construction costs

after 9 years [37]. Fig. 1 also illustrates this, where the 4× higher maintenance costs associated with ballasted track partially justify the policy of adopting a slab track solution. Typically slab track systems are considered to be cost-effective if the initial cost is less than 30% greater than that of ballasted track [52].

Under repeated train passages, railway tracks settle differentially along the line due to dynamic train-track interaction and variable track support conditions in the longitudinal direction [21]. This deterioration in vertical track geometry results in a cycle of increased train-track dynamic interaction forces and further track deterioration. These longitudinal track irregularities evolve with each load passage, meaning the characteristics of the train-track dynamic interaction forces, track stress distributions and settlements evolve over time. Regarding ballasted track, tamping can be used to restore track geometry, however this is not possible for slabs. Instead, for slab tracks, if the total settlement is within

* Corresponding authors.

E-mail addresses: cncc@leeds.ac.uk (C. Charoenwong), d.connolly@leeds.ac.uk (D.P. Connolly).

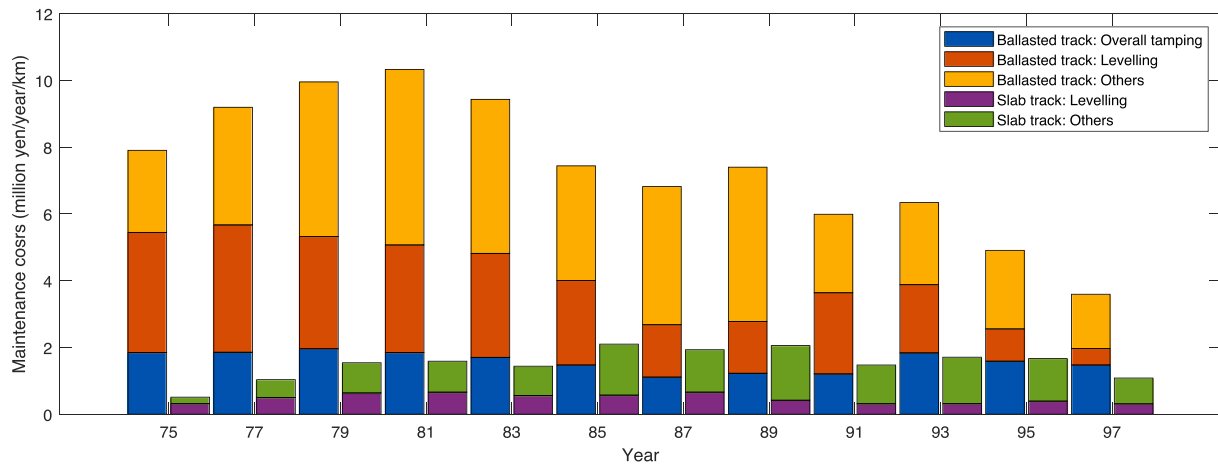


Fig. 1. Japanese HSR – Sanyo Shinkansen: maintenance costs (modified from [5]).

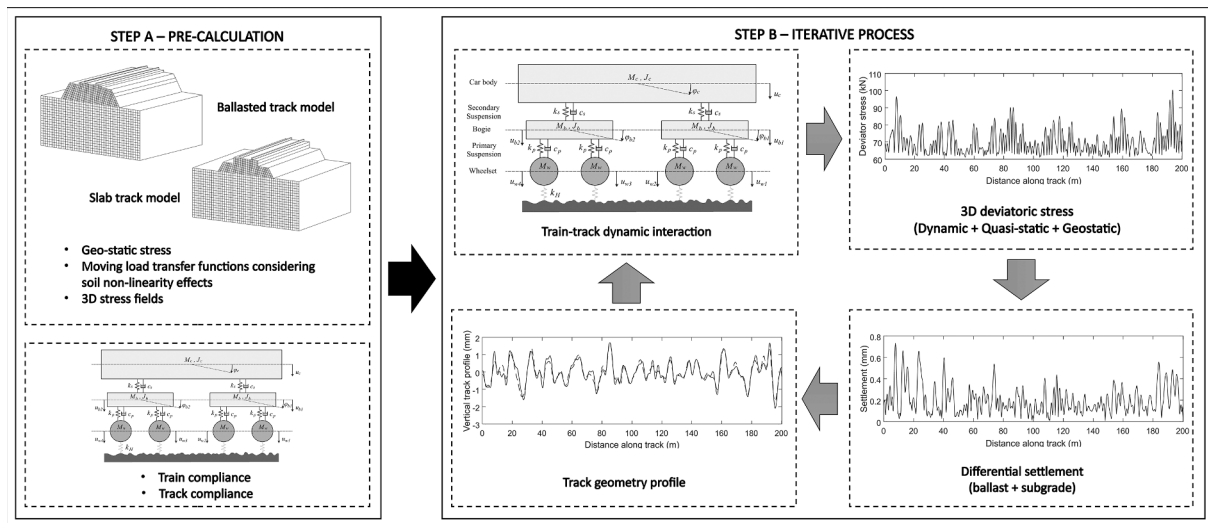


Fig. 2. Track differential settlement model overview.

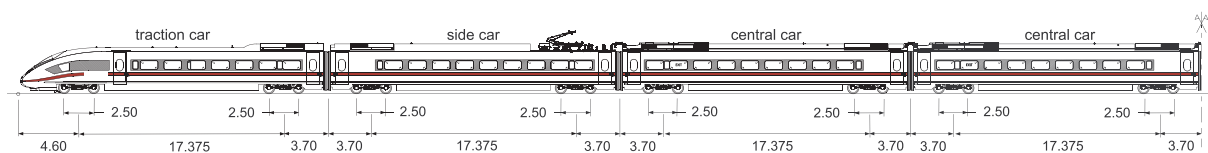


Fig. 3. ICE train wheelset layout dimensions (adapted from [29]).

a narrow range then adjustments can be made to the rail fasteners. To minimise the risk of settlements outside this narrow range during the slab track lifespan, settlements due to earthwork self-weight must also be minimised. Therefore slab tracks typically require more highly engineered foundations compared to ballasted track. This increases the construction cost difference between ballast and slab track-forms.

To predict differential track settlement due to train loading, methodologies have been proposed by [18,23,30,38], where an iterative train-passage simulation approach combined with settlement models is used to compute differential settlement in the ballasted track, considering changes in track geometry. Considering slab track settlement, a similar iterative simulation approach has been studied by [24,46] to predict the evolution of differential subgrade settlement. However, modelling cyclic loading in the time domain can require significant computational effort, and is thus challenging when calculating the 3D

dynamic stress fields in the track and ground over a large number of loading cycles [4,12,15,14,22,40]. It is also important that the distribution of track-ground stresses is modelled explicitly because deviatoric stress is one of the most influential parameters when computing settlement [33].

Two fundamental parts of a generalised railway settlement prediction model are first calculating the stress/strain response of the structure, and secondly calculating the corresponding settlement. Regarding settlement calculation, two common modelling approaches for calculation are constitutive [17,25,27,44,50,51] and empirical [26,33,32,34,36,39,43,45,47,54]. The constitutive approach often requires higher computational effort and a non-trivial number of material input properties that are difficult to quantify, thus making real-life application challenging [11,46]. An alternative modelling approach is to use empirical equations which have fewer input parameters and

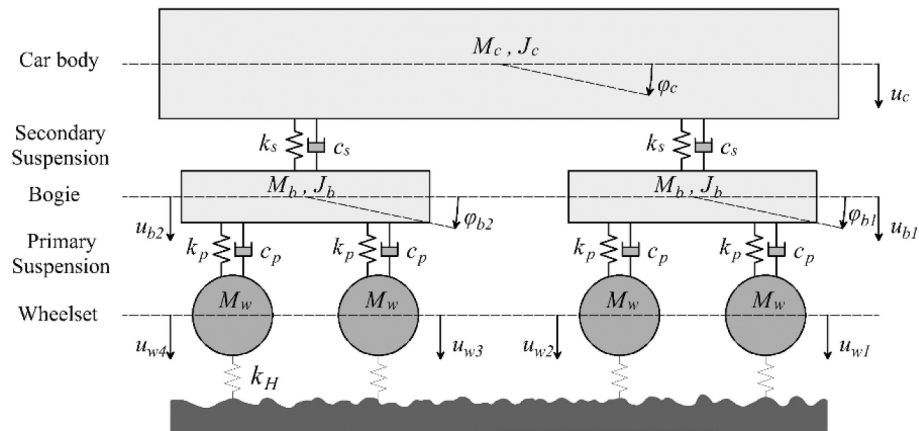


Fig. 4. Multi-body vehicle model of the ICE train.

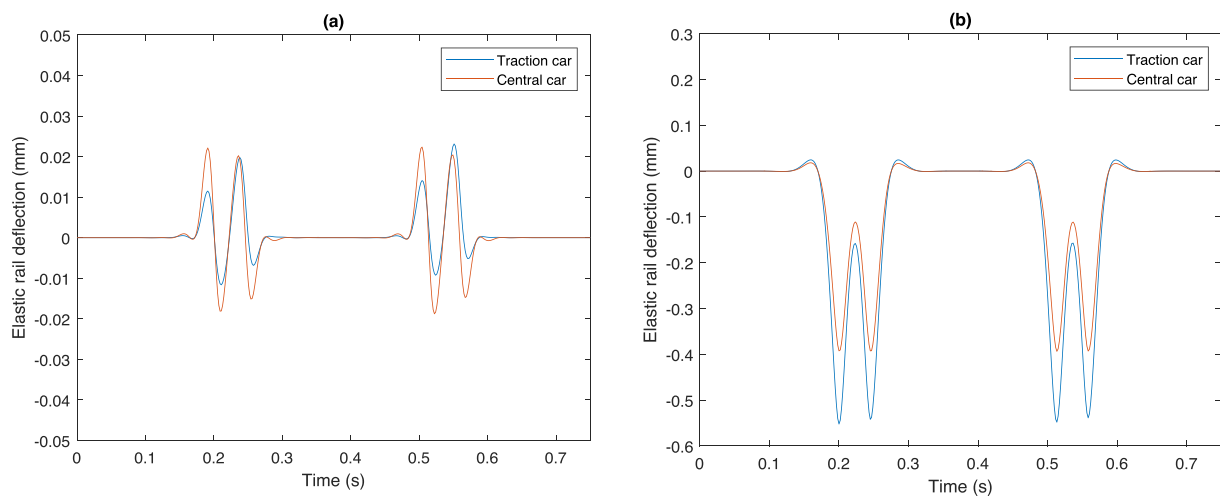


Fig. 5. Rail deflection, traction car Vs central car: (a) dynamic excitation, (b) combined quasi-static and dynamic excitation.

Table 1

ICE vehicle parameters.

Parameter	Symbol	Traction cars	Side and central cars
Axle spacing (m)	–	2.5	2.5
Bogie spacing (m)	–	17.375	17.375
Car body mass (kg)	M_c	50,000	35,000
Car body pitching moment of inertia (kg.m ²)	J_c	1.03×10^6	2.16×10^3
Bogie mass (kg)	M_b	2840	5154
Wheelset mass (kg)	M_w	1600	1750
Bogie pitching moment of inertia (kg.m ²)	J_b	3.22×10^3	2.46×10^3
Primary suspension stiffness (Nm ⁻¹)	k_p	4.30×10^6	1.40×10^6
Primary suspension viscous damping (Nsm ⁻¹)	c_p	24×10^3	120×10^3
Secondary suspension stiffness (Nm ⁻¹)	k_s	1.43×10^6	0.45×10^6
Secondary suspension viscous damping (Nsm ⁻¹)	c_s	70×10^3	40×10^3

require minimal computation, which when used with care, can accurately replicate on-track settlement behaviour [42].

This paper presents a novel numerical algorithm to compute differential track settlement for both ballasted and slab track. Train-track interaction, vehicle dynamics and 3D stress field propagation are modelled explicitly. The computational efficiency of the implementation

is high even when using solid elements to capture 3D stress fields. It uses an equivalent-linear wavenumber finite element method coupled with empirical settlement relationships in a manner that allows for the track irregularities to evolve after every load passage, before applying the next load.

2. Numerical differential settlement model

2.1. Model overview

A 2-step coupled modelling strategy is used to compute differential track settlement and future track deterioration. The model is based on a FEM-PML (Finite Element Method with Perfectly Matched Layers) approach, solved in a hybrid manner, across both frequency-wavenumber and time-space domains. The 3D solution in the time-space domain is obtained by a double inverse Fourier transform applied to the frequency-wavenumber solution. The maximum wavenumber is set to 10 rad/m to cover all relevant waves within the frequency range of interest. 1024 wavenumbers are sampled over the range from -10 to +10 rad/m which is capable of capturing the peaks in the integrand while minimising computational effort. The two coupled steps are shown in Fig. 2: Step A, pre-calculation of transfer functions; and Step B, iterative settlement process. Considering repeated dynamic train loads, the proposed transfer function approach is well-suited because the track geometry profile can be updated after every load passage with minimal computational effort.



Fig. 6. Full scale ballast testing.

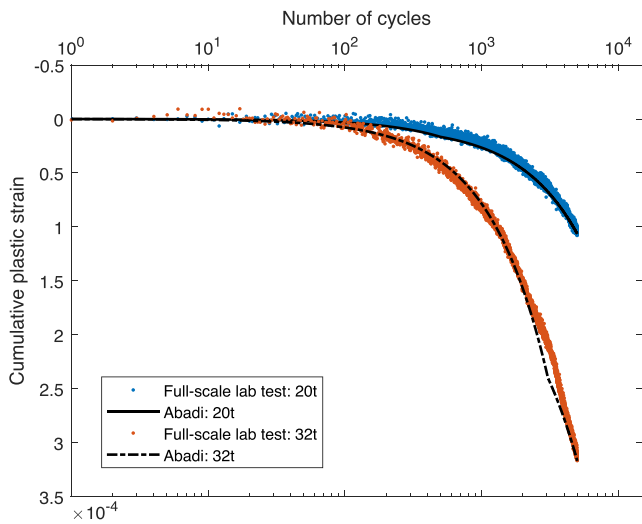


Fig. 7. Comparison of experimental lab data against published datasets.

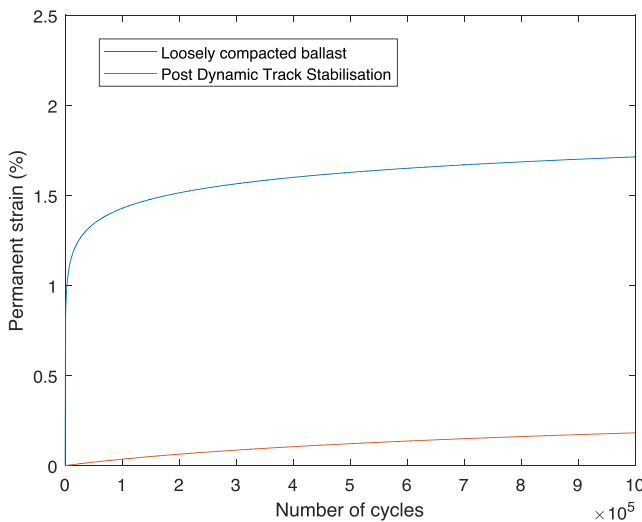


Fig. 8. Typical ballast settlement curves.

Table 2
Settlement material parameters.

Soil type	Reference	Settlement material parameter		
		a	b	m
Fat clay, CH	[33]	1.20	0.18	2.40
Lean clay, CL	[33]	1.10	0.16	2.00
Elastic silt, MH	[33]	0.84	0.13	2.00
Sand silt, ML	[33]	0.64	0.10	1.70
Sand gravel	[48]	0.52	0.15	1.49

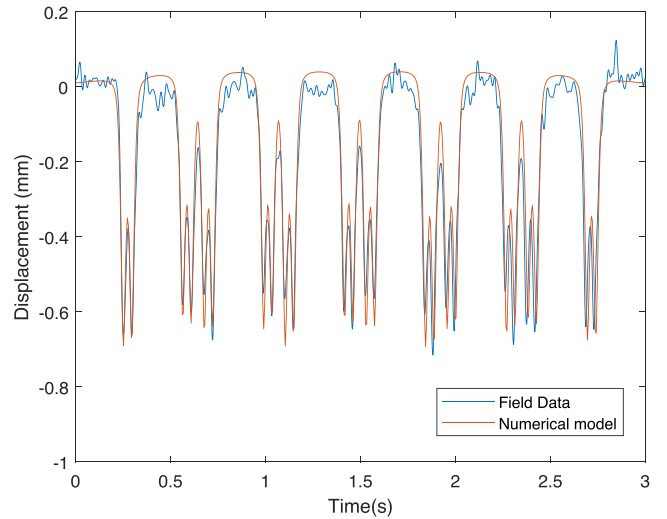


Fig. 9. Ballast track validation - Rail displacement time histories due to the train passage.

Step A is a pre-calculation step which involves computing the 3D elastodynamic response and the geo-static stresses in the track and ground. The moving load transfer function considering non-linear track-ground stiffness is computed in the frequency-wavenumber domain. The 3D stress transfer functions due to quasi-static and dynamic loading are then found. Several matrices required for computing the train-track dynamic interaction are also prepared in advance.

In Step B, an iterative solver is implemented using a combination of wavenumber-frequency and space-time domains. Based on the track irregularity profile, track compliance and rolling stock, the train-track

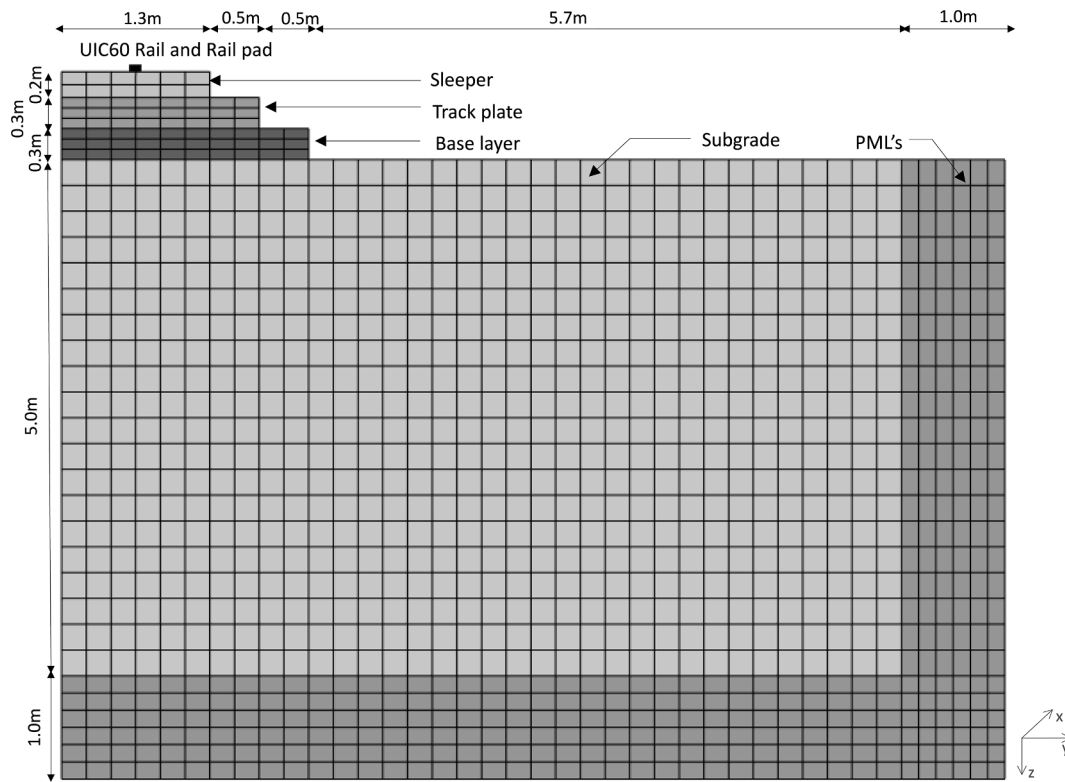


Fig. 10. Finite element mesh for slab track validation.

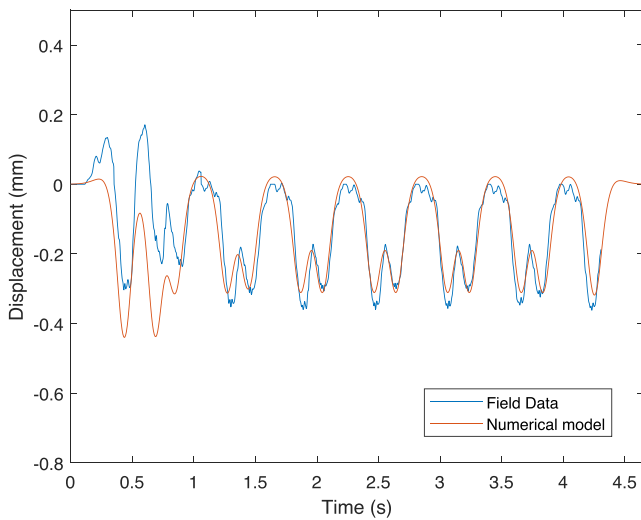


Fig. 11. Concrete slab track validation - displacement time histories measured at the track plate centre.

dynamic interaction force is calculated using a multi-body model. The total deviatoric stress (combined quasi-static, dynamic and geo-static) and settlements in the track and the ground are then calculated over the entire model track length in the direction of train passage. The vertical track geometry profile is updated after every axle passage and thus the train-track dynamic force and deviatoric stress are also recalculated at each iteration. These steps are repeated for the desired number of cycles, or until a threshold limit value is reached (e.g. as defined by international/national standards). It should be noted that due to the pre-calculations performed in Step A, each Step B iteration requires minimal computational effort, thus allowing for the rapid simulation of many axle passages. Additional information regarding the

numerical model can be found in [9,10].

2.2. Track-ground simulation

The track and the ground are modelled using 8-node 2.5D finite elements. Perfectly Matched Layers (PML) are used as absorbing boundaries for the unbounded ground regions. The 2.5D method assumes invariant geometry in the direction of train passage, however the sleepers are discontinuous elements. Therefore, the sleepers are modelled as continuous and orthotropic elements, where the physical properties of the sleepers are used in the cross-section [3,28]. To do so, in the longitudinal plane, the stiffness is set close to zero. Therefore, the elasticity matrix $[D]_{sleeper}^{-1}$ in Eq. (1) is used to simulate the sleeper elements where the shear modulus in the isotropic YZ plane, G_{kk} is defined by Eq. (2):

$$[D]_{sleeper}^{-1} = \begin{bmatrix} \frac{1}{E_x} & \frac{\nu_{xk}}{E_k} & \frac{\nu_{xk}}{E_k} & 0 & 0 & 0 \\ \frac{\nu_{xk}}{E_x} & \frac{1}{E_x} & \frac{\nu_{kk}}{E_k} & 0 & 0 & 0 \\ \frac{\nu_{xk}}{E_x} & \frac{\nu_{kk}}{E_k} & \frac{1}{E_x} & 0 & 0 & 0 \\ 0 & 0 & 0 & \frac{1}{G_{xk}} & 0 & 0 \\ 0 & 0 & 0 & 0 & \frac{1}{G_{kk}} & 0 \\ 0 & 0 & 0 & 0 & 0 & \frac{1}{G_{xk}} \end{bmatrix} \quad (1)$$

$$G_{kk} = \frac{E_k}{2(1 + \nu_{kk})} \quad (2)$$

where E_k is the Young's modulus of the sleepers in the isotropic YZ plane; ν_{kk} is Poisson's ratio of the sleeper in the isotropic YZ plane; G_{kk} is

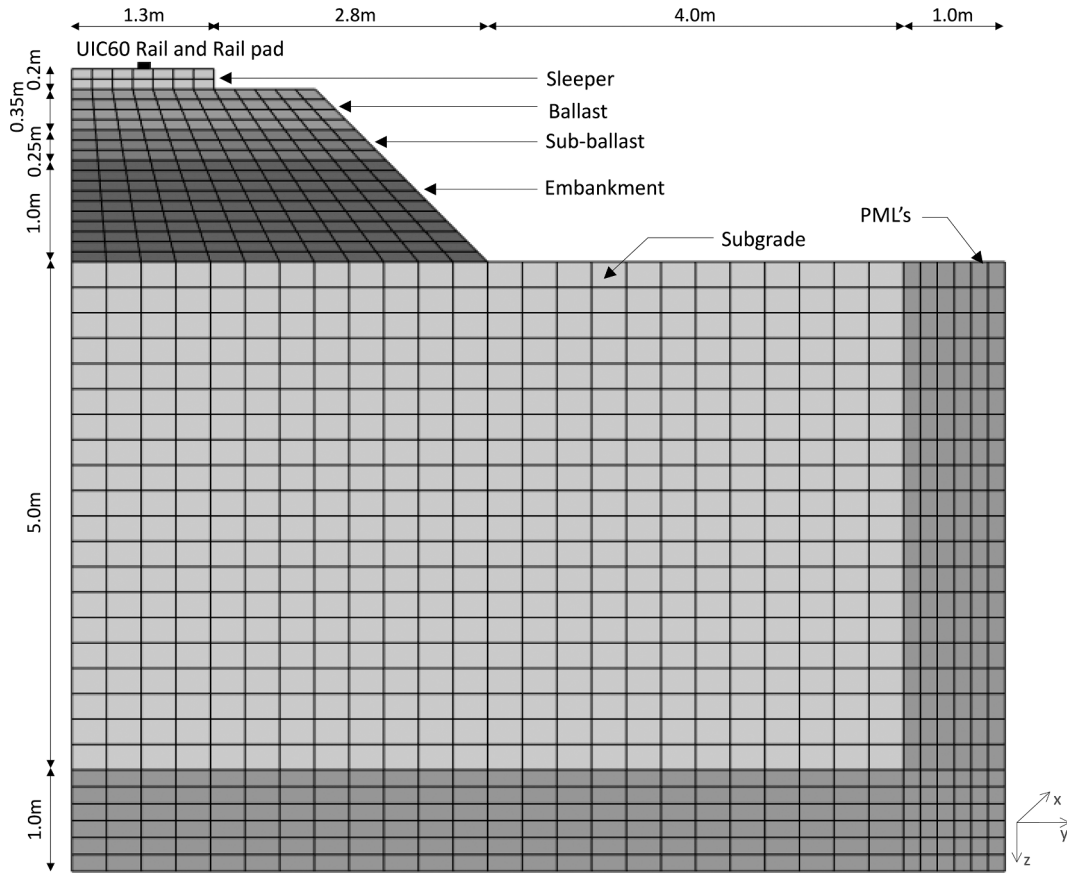


Fig. 12. Finite element mesh of ballasted track.

the shear modulus in the isotropic YZ plane; E_x is Young's modulus of the sleepers in the track direction; ν_{xk} is Poisson's ratio of the sleeper in the track direction; and G_{xk} is the shear modulus in the track direction.

The railpads are modelled using spring elements for both ballasted track and slab track models. As the rail is discretely supported by railpads at 0.65 m spacing, the equivalent continuous railpad stiffness is calculated from its discrete nature using Eq. (3):

$$K_{continuous} = \frac{K_{discrete}}{\text{Sleeper spacing}} \quad (3)$$

2.3. Train-track interaction

A complete 2D vehicle which takes into account the main structural aspects of the train dynamics [55] is adopted in this study. Vehicle-track interaction is solved using a compliance procedure formulated in a moving frame of reference, subject to a moving train [13,16]. Considering the ICE train used in this analysis, Fig. 3 shows the vehicle dimensions, while the rigid multi-body vehicle formulation with two levels of suspension is shown in Fig. 4. The analysis is performed in the frequency domain considering the transformation of the space-domain track profile. The formulas for the dynamic interaction force in the frequency domain are given by Eqs. (4)-(10). Regarding the Hertzian stiffness, a linearization procedure is adopted, in which only the dead load transmitted by the wheelset is taken into account when deriving a representative value [29].

$$\{F_{dyn}(\Omega)\} = -([V] + [V^H] + [T])^{-1} \{\Delta u(\Omega)\} \quad (4)$$

$$\{\Delta u(\Omega)\} = \delta u\{b(\Omega)\} \quad (5)$$

$$b(\Omega)_i = e^{i2\pi\Omega t_i} \quad (6)$$

$$T(\Omega) = \frac{1}{2\pi} \int_{-\infty}^{+\infty} u_c^G(k_x, \omega) dk_x \quad (7)$$

$$V^H = \frac{1}{k_H} \quad (8)$$

$$k_H = \frac{3}{2G} P_0^{1/3} \quad (9)$$

$$V(\Omega) = [Z]([K^v] - \Omega^2[M^v])^{-1}[Z]^T \quad (10)$$

In Eqs. (4)-(10), Ω is the driving frequency, defined by $\Omega = \frac{2\pi}{\lambda} v_0$; T is the flexibility term of the track compliance; V is the flexibility term of the vehicle compliance; V^H is the contact flexibility matrix; k_H is the linearised (Hertzian) contact stiffness; P_0 is the static load transmitted by the wheel to the rail; G is the contact constant depending on the radius and geometry of the wheel, and rail bearing surface; Z is a constant matrix, M^v is the vehicle mass matrix and K^v is the vehicle stiffness. The mass and stiffness matrices of the vehicle system with primary and secondary suspensions can be found in [9,10].

Regarding track irregularities, the profile can be described using power spectral density (PSD) as a function of spatial frequency, of which there are various formulations. The formulation used in this work is based on the Federal Railway Administration (FRA) which divides the track into different classes for the quantification of track unevenness [20]. The formulation based on FRA has the Eqs. (11) to (13):

$$S_n(k_x) = \frac{Ak_3^2(k_x^2 + k_2^2)}{k_x^4(k_x^2 + k_3^2)} \quad (11)$$

where the spatial frequency is $k_x = \frac{2\pi}{\lambda_{irr}}$, λ_{irr} is the wavelength of the ir-

Table 3
Ballasted track properties.

Component	Parameter	Value	
UIC 60 Rail (single rail)	Height (m)	0.172	
	Length in transversal direction (m)	0.015	
	Section area (m ²)	7.677 × 10 ³	
	Moment of Inertia y-y (m ⁴)	3.038 × 10 ⁻⁵	
	Moment of Inertia z-z (m ⁴)	0.512 × 10 ⁻⁵	
	Young's modulus (MPa)	2.11 × 10 ⁵	
	Density (kg/m ³)	7850	
	Poisson's ratio	0.3	
	Railpad (spring element)	Hysteric damping coefficient	0.01
		Continuous stiffness (N/m ²)	200 × 10 ⁶
Viscous damping (Ns/m ²)		22.5 × 10 ³	
Sleeper (G44)	Height (m)	0.2	
	Length in transversal direction (m)	2.5	
	Sleeper spacing (m)	0.65	
	Young's modulus (MPa)	3 × 10 ⁴	
	Density (kg/m ³)	2500	
	Poisson's ratio	0.2	
	Hysteric damping coefficient	0.01	
Ballast	Height (m)	0.35	
	Length in transversal direction (m)	2.8	
	Young's modulus (MPa)	220	
	Density (kg/m ³)	1600	
	Poisson's ratio	0.12	
	Hysteric damping coefficient	0.06	
	Sub-ballast (Sand gravel)	Height (m)	0.25
		Length in transversal direction (m)	3.5
		Young's modulus (MPa)	210
		Density (kg/m ³)	2000
Poisson's ratio		0.3	
Hysteric damping coefficient		0.05	
Settlement parameter a		0.52	
Settlement parameter b		0.15	
Settlement parameter m		1.49	
Compressive strength (kPa)		350	
Embankment (Sand gravel)	Height (m)	1.0	
	Young's modulus (MPa)	200	
	Density (kg/m ³)	2000	
	Poisson's ratio	0.3	
	Hysteric damping coefficient	0.05	
	Shear wave speed (km/h)	706	
	Settlement parameter a	0.52	
	Settlement parameter b	0.15	
	Settlement parameter m	1.49	
	Compressive strength (kPa)	320	
Subgrade (Silt)	Young's modulus (MPa)	100	
	Density (kg/m ³)	2000	
	Poisson's ratio	0.35	
	Hysteric damping coefficient	0.03	
	Shear wave speed (km/h)	547	
	Settlement parameter a	0.64	
	Settlement parameter b	0.1	
	Settlement parameter m	1.7	
	Compressive strength (kPa)	240	

regularity, A is a roughness constant, and k_2 and k_3 are spatial frequency constants.

After computing the PSD, the amplitude of unevenness in terms of the spatial frequency is:

$$\delta u_j = \left(\sqrt{2S_n(k_x)} \Delta k_x \right) e^{-i\theta_j} \quad (12)$$

where Δk_x is the resolution retained for the spatial frequency, and θ is phase angle, taken as a random variable with uniform distribution in the range 0-2 π . The metric considered for threshold exceedance is the standard deviation over a 200 m track length. Therefore the initial track profile in terms of position x is obtained using:

$$u_{irr}(x) = \sum_{j=1}^N \delta u_j e^{ik_{x_j} x} \quad (13)$$

It has been shown that the dynamic train-track response and track

settlements are most accurately replicated when full-car rolling-stock models are simulated [9,10]. However, as common with many high speed rolling stock, the ICE trainset is comprised of cars with 3 differing sets of properties (Fig. 3). To simplify the trainset the 'side' car properties are changed to be equal to the 'central' cars, due to their high similarity [29].

Fig. 5 shows the relationship between the track response due to both central and traction cars. For the purpose of the illustration, a 2D model based on beam on elastic foundation theory [31] is used. An infinite Euler-Bernoulli beam is used to represent the rail which is supported by a single continuous elastic layer. It has the following material properties (single rail): Young's modulus 2.1×10^{11} N/m²; second moment of area 30.55×10^{-6} m⁴; cross section area 0.00763 m²; density 7850 kg/m³; and support stiffness 100×10^6 N/m². An artificial track irregularity profile for wavelengths in the range $3 < \lambda \leq 25$ m is generated using the PSD (Power Spectral Density) function defined by FRA [20] but the constants modified to generate specific SD profiles at speed of 200 km/h. The properties of vehicles are based upon the ICE [29] as shown in Table 1.

Fig. 5(a) shows track displacements due to dynamic excitation between a traction car and a central car. The central car model results in a higher dynamic response, however the traction car model results in higher overall displacement (considering both quasi-static and dynamic loads) as shown in Fig. 5(b). Therefore, both traction and side/central models are taken into account in the 2.5D train-track interaction and settlement simulation. This is done by running the model in the order of train cars: Traction*2; Central*6; Traction*2; Central*6...etc.

2.4. Ballast and subgrade settlements

2.4.1. Ballast settlement

Full-scale laboratory tests were performed using the apparatus described in [19,35,41] and shown in Fig. 6. A single sleeper was cyclically loaded with the equivalent of 20 t and 32 t axle loads. A 20 t axle load represents a fully loaded passenger train, while a 32 t axle load represents a heavy freight train [29]. A G44 concrete sleeper was tested, supported by a 0.4 m depth of ballast and a 0.18 m depth of well-compacted granular material. To replicate train loading, a sinusoidal loading function was applied at a frequency of 2 Hz. Deformation was measured using linear variable differential transformers, placed on the sleeper and sampled at 200 Hz. Fig. 7 compares the experimental data against the data in the literature [1] with removal of the permanent strain during initial cycles. It is shown that the settlement rates are similar for both 20 and 32 tonne tests.

To fit curves to the experimental results, an ORE-type formulation [39] is used. The ballast permanent strain per loading increment is computed using eq. (14).

$$\begin{aligned} \Delta \varepsilon_{p-b,i} &= 0.375 (\sigma_{d-b,i}^2) \times [\alpha_1 - \alpha_2] \\ \text{where} \\ \alpha_1 &= 1 + 0.4 \log_{10}((dN(i)) + N_{lb}) \\ \alpha_2 &= 1 + 0.4 \log_{10}((dN(i-1)) + N_{lb}) \end{aligned} \quad (14)$$

where $\Delta \varepsilon_{p-b,i}$ = ballast permanent strain increment; $\sigma_{d-b,i}$ = ballast deviatoric stress updated every iterative step (in MPa); dN = the repeated of load application for each iterative step; i = iterative step; and N_{lb} = the number of load cycles after the last ballast renewal/tamping.

The derived settlement equations are then modified to account for the differences in ballast compaction achievable in a laboratory setting versus a full-scale railway construction. An important difference between these compacted states is the application of Dynamic Track Stabilisation, commonly used on new lines particularly at higher speeds [49]. Dynamic Track Stabilisation is often considered to provide the equivalent compactive effort as 100,000 tonnes. Therefore Fig. 8 shows the unmodified ballast settlement curve and the modified settlement curve assuming the ballast has already received these loading cycles

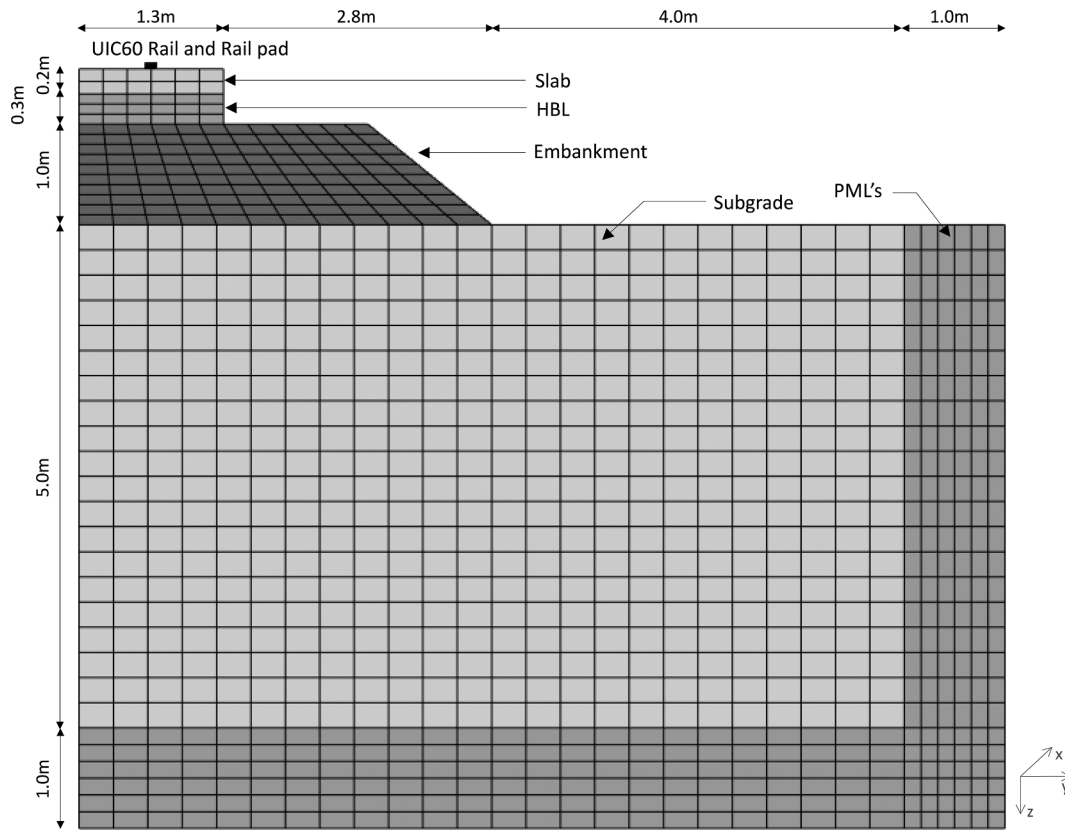


Fig. 13. Finite element mesh of slab track.

Table 4
Slab track properties.

Component	Parameter	Value
Slab	Height (m)	0.25
	Length in transversal direction (m)	2.6
	Young's modulus (MPa)	3×10^4
	Density (kg/m ³)	2500
	Poisson's ratio	0.2
HBL	Hysteric damping coefficient	0.001
	Height (m)	0.3
	Length in transversal direction (m)	2.6
	Young's modulus (MPa)	10×10^3
	Density (kg/m ³)	2500
	Poisson's ratio	0.2
	Hysteric damping coefficient	0.03

before experiencing live traffic.

2.4.2. Subgrade settlement

The subgrade permanent strain increment per loading is computed using Eq. (15) which is a modified version of that proposed by Li and Selig [33].

$$\Delta \epsilon_{p-s,i} = \frac{a}{100} \left(\frac{\sigma_{d-s,i}}{\sigma_s} \right)^m \left[((dN(i) + N_{ls})^b - ((dN(i-1) + N_{ls})^b) \right] \quad (15)$$

where $\Delta \epsilon_{p-s,i}$ = subgrade permanent strain increment; $\sigma_{d-s,i}$ = subgrade deviatoric stress updated every iterative step (in Pa); σ_s = soil compressive strength (in Pa); N_{ls} = the number of load cycles after the last subgrade renewal; and a , m , and b = material parameters given in Table 2.

2.5. Model validations for short-term prediction

2.5.1. Ballasted track

The ballasted track model is validated against the experimental field data from a railway line near the town of Carregado in Portugal. The rolling stock is an Alfa-Pendular train composing of 6 vehicles, moving at 219 km/h [2]. Regarding the geometric properties of the model, the finite element mesh of ballasted track is similar to Fig. 12 but consists of ballast and sub-ballast on top of 10 soil layers supported by bedrock. The heights of ballast and sub-ballast are 0.57 and 0.55 m respectively. The ballast has the following material properties: Young's modulus 97MPa; Poisson's ratio 0.27; and density 1590 kg/m³. The same parameters but for sub-ballast are 212MPa, 0.3, and 1910 kg/m³.

Fig. 9 compares the rail displacements in the time domain between the simulation and the field measurement. There is a strong match between the simulated and measured results, in terms of both magnitude and timing of response.

2.5.2. Slab track

A slab track model is validated against the measurement data of slab track displacements under train passages [7]. The track consists of sleepers on a concrete track plate, and base layer on top of a soil layer (see Fig. 10). The soil has a shear wave velocity of 100m/s, a density of 2000kg/m³, and a Poisson's ratio of 0.33. The Young's modulus of the track plate and the base layer are 3×10^{10} and 5×10^9 Pa respectively [7,6].

The displacement time histories measured at middle of track plate from the simulation and the measurement are compared as shown in Fig. 11. The responses are due to the passage of an ICE train with a locomotive and 6 carriages, moving at 160 km/h. The agreement is strong between the predicted and measured values in terms of magnitude and timing of response. The central carriages provide a closer response than the first cars. This is most likely because the original

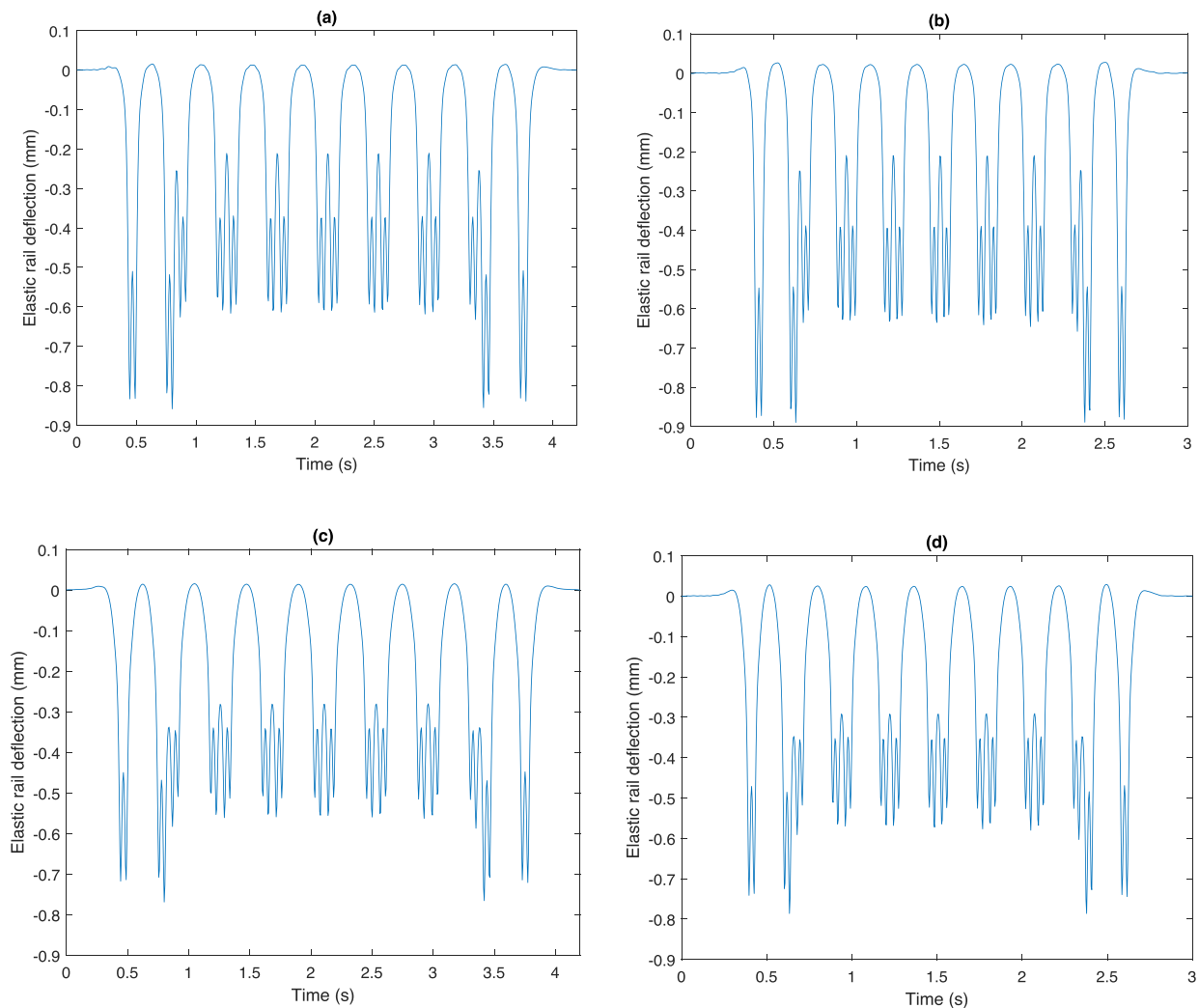


Fig. 14. Track deflection time histories considering both quasi-static and dynamic excitation: (a) Ballasted track-200 km/h (b) Ballasted track-300 km/h (c) Slab track-200 km/h (d) Slab track-300 km/h.

measurements were recorded using accelerations and double integrating such signals is a longstanding railway challenge, which causes a drift in the measurement datum. This can be seen in the field data where the data appears to have been shifted upwards despite the track experiencing a heavier axle load.

3. Case studies

3.1. Track parameters

3.1.1. Ballasted track

The finite element mesh of the ballasted track case study is shown in Fig. 12. The characteristics of the rails, rail pads, sleepers, ballast, sub-ballast, embankment and subgrade are described in Table 3. The track is assumed to be newly constructed using modern compaction techniques, with new, unfouled ballast that has been subject to dynamic track stabilisation.

3.1.2. Slab track

The finite element mesh of slab track is shown in Fig. 13. The rails, rail pads, embankment and subgrade have the same characteristics as those in the ballasted track, whereas the characteristics of slab and HBL (hydraulically bound layer) are described in Table 4.

3.2. Track geometry profile and traffic parameters

The initial track irregularity profile for both tracks is artificially generated using the PSD function defined by [20], considering 40 frequencies. The values of parameters A , k_2 and k_3 are set as $0.053 \times 10^{-6} \text{ m}^2 \text{ rad/m}$, $14.639 \times 10^{-2} \text{ rad/m}$ and $82.474 \times 10^{-2} \text{ rad/m}$, resulting in a track geometry profile with a starting standard deviation (SD) of 0.4 mm. The rolling stock is an 8-car ICE with 2 traction cars and 6 central cars, equating to 32 axles per train. Considering the traffic volume in terms of milling gross tons (MGT), a single ICE train is equal to 0.0005MGT. Therefore, the traffic volume of 1MGT is equivalent to 2000 train passages, or 64k axle passages.

4. Results

This section presents the elastic track deflection time histories, followed by the settlement behaviour shortly after the line is opened. Next the degradation of track geometry over a longer time period is analysed (30MGT). Finally, the deviatoric stresses with the track layers are presented.

4.1. Track deflection time histories

Considering the full ICE train with both quasi-static and dynamic excitation, Fig. 14 compares elastic track deflection time histories for

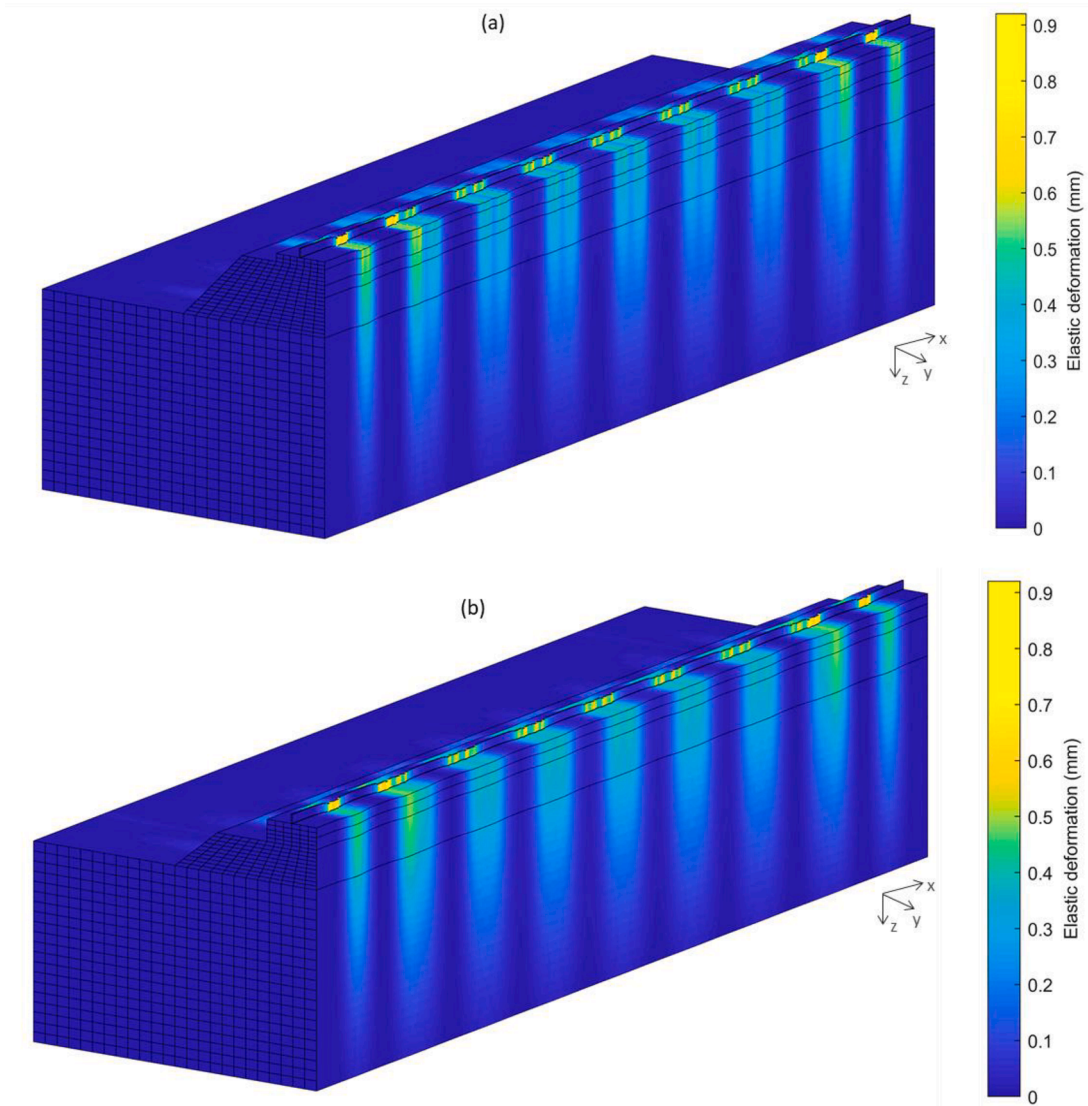


Fig. 15. 3D track-ground deflection profile (slice along track centreline considering both quasi-static and dynamic excitation): (a) ballasted track (b) slab track.

ballasted and slab tracks. Fig. 14(a) and (b) compare elastic track deflection time histories of the ballasted track at moving speeds of 200 and 300 km/h. It is seen that the higher speed induces larger elastic deflection. Similar trend are also visible with the slab track when increasing moving speed as shown in Fig. 14(c) and (d). Comparing the ballasted track and slab track subject to the same moving speeds, the elastic deflections in the ballasted track are marginally higher than in slab track. This is true at both 200 and 300 km/h.

Fig. 15(a) and (b) illustrate the 3D track-ground displacement contours for ballasted and slab tracks at 300 km/h and the response propagating from the rail into supporting track-ground structure. Note that although the domain shown is the full 200 m track section with a 184.9 m long train, to maximise viewability, the x-axis is scale is scaled by a factor of 8 compared to the y and z-axis.

4.2. Early life settlement

To investigate early life settlement, the differential settlement evolution over 100k axle passages is shown in Fig. 16. Fig. 16 (a) and (b) show the vertical track geometry profiles of both ballasted and slab tracks at the instant they reach 100k load cycles for the speeds of 200 and 300 km/h respectively.

Fig. 17 compares the evolution of geometry SD over number of load

cycles from the initial SD value until 100k load passages for four cases: ballasted track at speed of 200 km/h, ballasted track at speed of 300 km/h, slab track at speed of 200 km/h and, slab track at speed of 300 km/h. The corresponding SD at 100k axle passages are summarised in Table 5. At a speed of 200 km/h, the SD of ballasted and slab tracks are 0.463 and 0.430 mm respectively. This corresponds to a 7.13% decrease for the slab track. At speed of 300 km/h, the SD of ballasted and slab tracks increases to 0.471 and 0.431 mm respectively, corresponding to marginally higher 8.49% decrease.

4.3. Settlement after 30MGT of traffic

To simulate differential settlement evolution over a longer-term, both ballasted and slab tracks are now subjected to 30MGT traffic. Fig. 18(a) and (b) show the vertical track geometry profiles of both ballasted and slab tracks at the moment of reaching 30MGT for the speeds of 200 and 300 km/h respectively.

Fig. 19 compares the evolution in geometry SD with MGT from the initial 0.4 mm SD value for ballasted and slab tracks, considering both moving speeds. The results are summarised in Table 6. The SD of ballasted and slab tracks at 200 km/h are 1.272 and 0.989 mm respectively, which correspond to a 22.25% decrease. At a moving speed of 300 km/h, the SD of ballasted and slab tracks increases to 1.525 and 1.008 mm

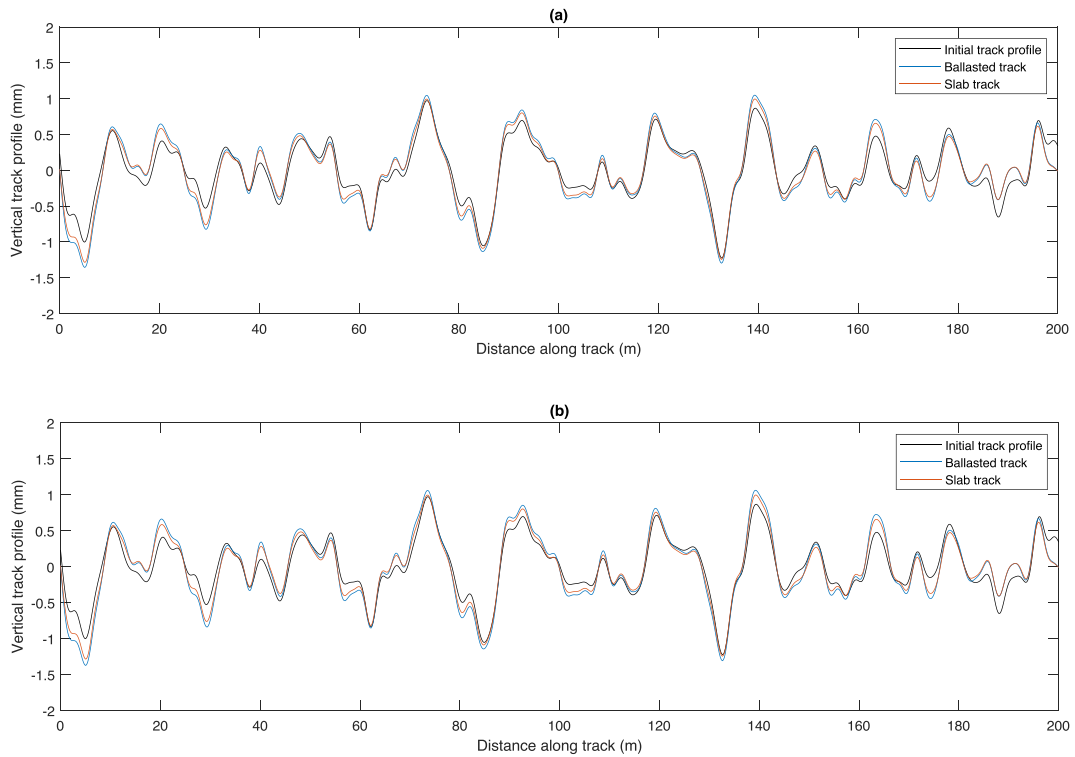


Fig. 16. Vertical track profiles after 100k axle passages for ballasted track and slab track: (a) 200 km/h (b) 300 km/h.

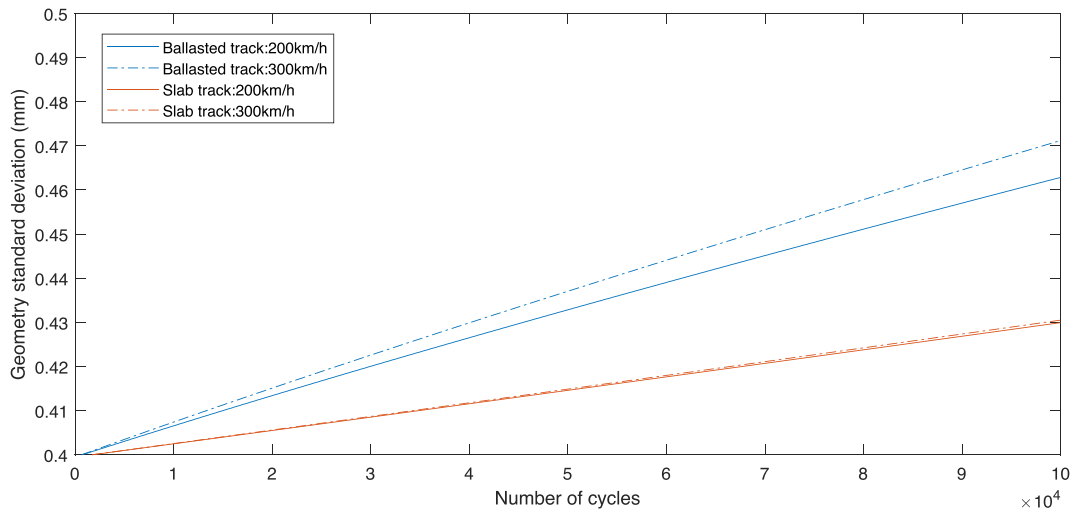


Fig. 17. Geometry SD curves over 100k load passages for ballasted track and slab track.

Table 5
Geometry SD after 100k axle passages for ballasted track and slab track.

Speed (km/h)	Track type	SD after 100k axle passages (mm)	Percentage decrease
200	Ballasted track	0.463	7.13%
	Slab track	0.430	
300	Ballasted track	0.471	8.49%
	Slab track	0.431	

respectively, corresponding to a 33.90% decrease. Note that at the maximum operational linespeed of 300 km/h, the SD threshold limit for ballasted track tamping maintenance is approximately 1.5 mm [53]. Therefore the ballasted track at 300 km/h linespeed requires tamping prior to 30MGT, while the 200 km/h ballast track does not.

4.4. Deviatoric stresses within track-bed and subgrade layers

Deviatoric stress is one of the most influential parameters on settlement [33]. Therefore the contribution of deviatoric stresses along the depths of the track-bed and subgrade layers are investigated. The definition of track-bed layers in this work is ballast, subballast and embankment for the ballasted track, and only the embankment for the slab track. The deviatoric stresses due to the vehicle's quasi-static and

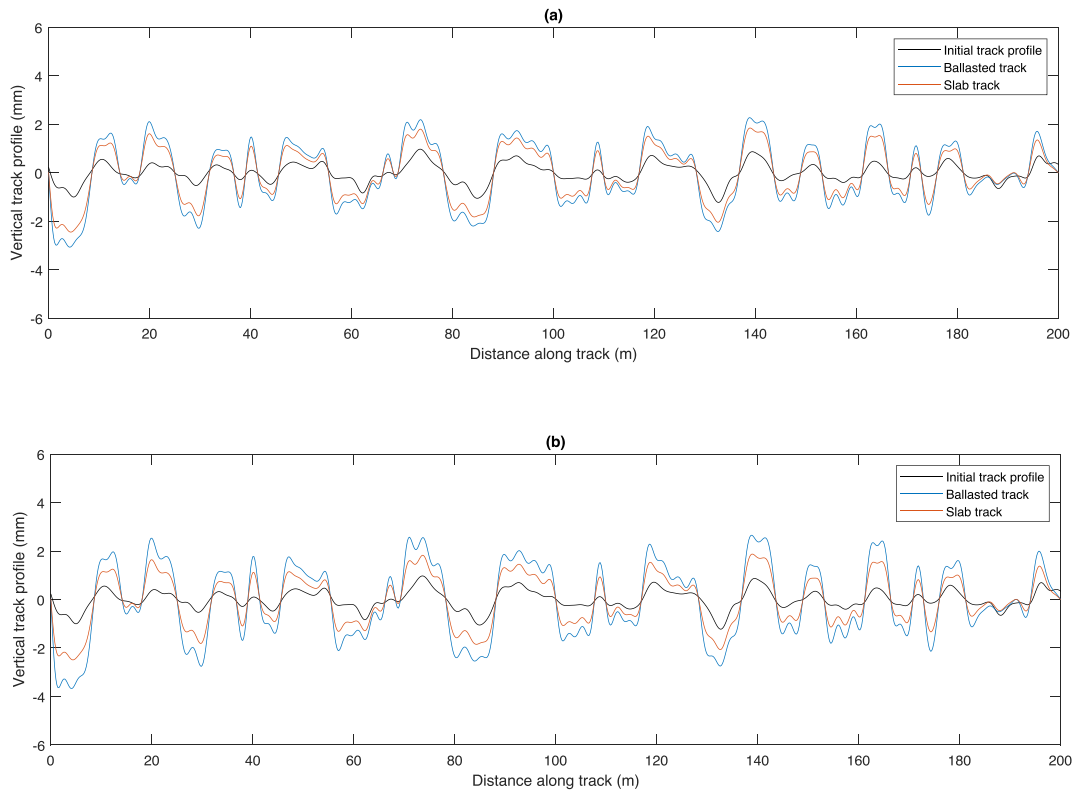


Fig. 18. Vertical track profiles after 30MGT traffic for ballasted track and slab track: (a) 200 km/h (b) 300 km/h.

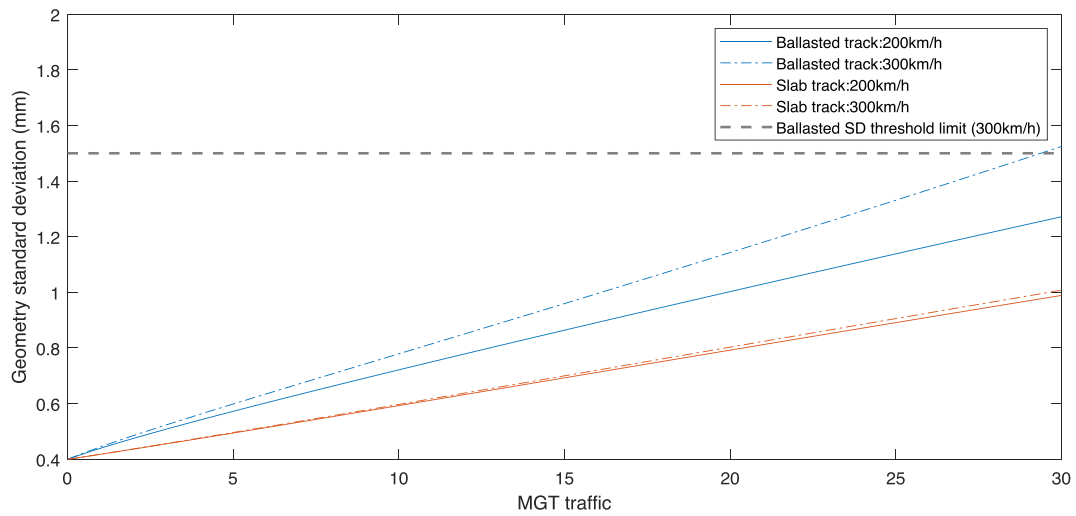


Fig. 19. Geometry SD curves over 30MGT traffic for ballasted track and slab track: (a) 200 km/h (b) 300 km/h.

Table 6
Geometry SD after 30MGT traffic for ballasted track and slab track.

Speed (km/h)	Track type	SD after 30MGT traffic (mm)	Percentage difference
200	Ballasted track	1.272	22.25%
	Slab track	0.989	
300	Ballasted track	1.525	33.90%
	Slab track	1.008	

dynamic loading components are compared. The quantities are calculated at the track centreline considering a ICE central car and selecting the mean deviatoric stresses over the track length.

Considering track-bed layers, the contribution of deviatoric stresses within the ballasted track are shown in Fig. 20(a) considering quasi-static excitation and Fig. 20(b) considering dynamic excitation. Similar to the ballasted track, the contribution of deviatoric stresses due to the quasi-static and dynamic excitations within the embankment for the slab track are shown in Fig. 21(a) and (b) respectively. Considering the subgrade layer of both ballasted and slab tracks, the quasi-static and dynamic deviatoric stresses are shown in Fig. 22(a) and (b) respectively.

It's seen in Fig. 20(a), Fig. 21(a) and Fig. 22(a) that the quasi-static deviatoric stresses in both the ballasted and slab track increase with

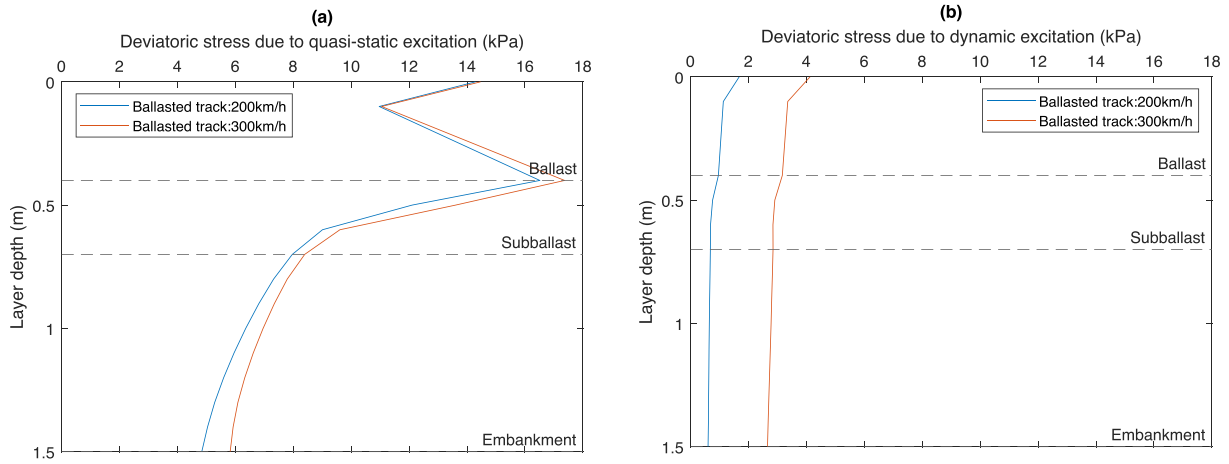


Fig. 20. Deviatoric stresses within the track-bed of ballasted track: (a) quasi-static excitation (b) dynamic excitation.

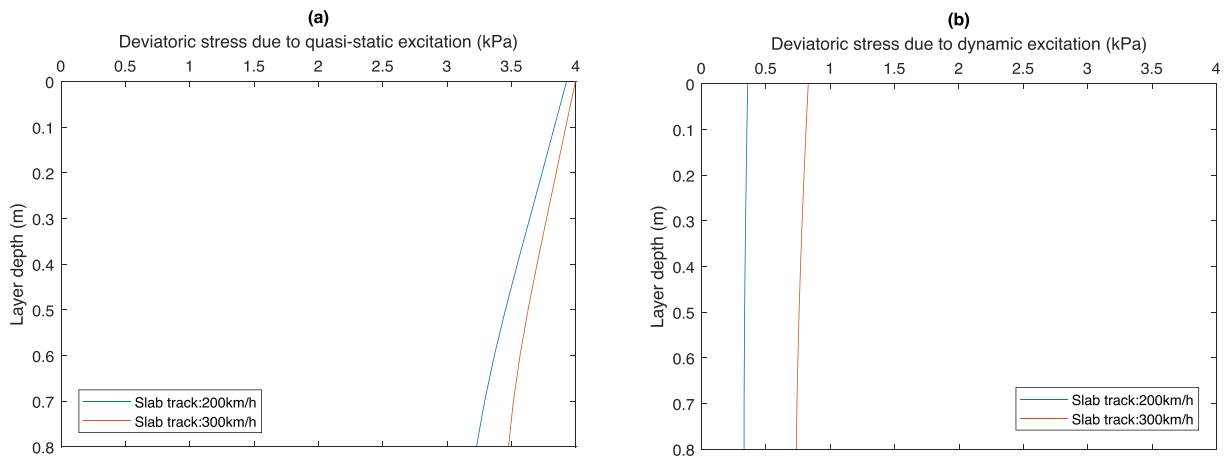


Fig. 21. Deviatoric stresses within the track-bed of slab track: (a) quasi-static excitation (b) dynamic excitation.

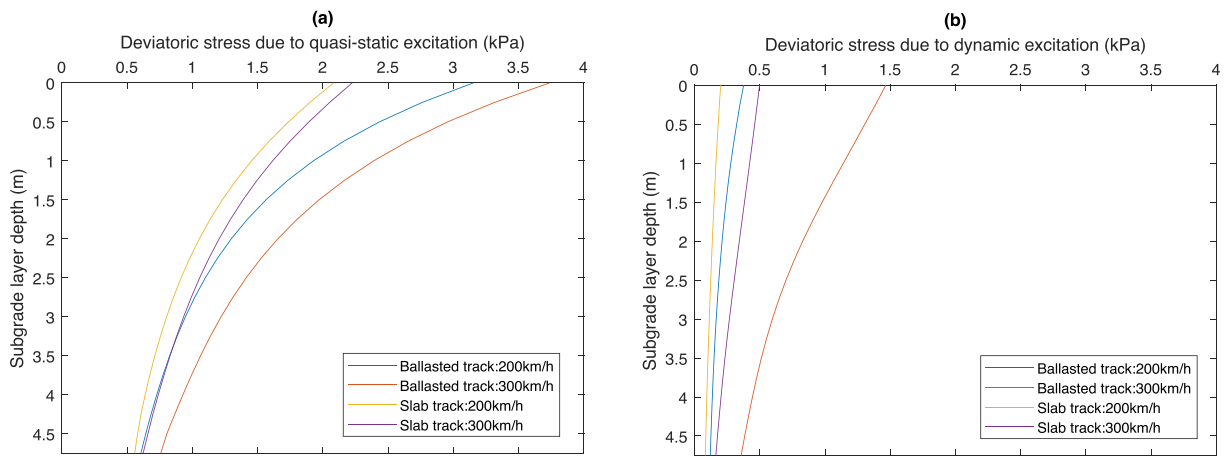


Fig. 22. Deviatoric stresses within the subgrade layer: (a) quasi-static excitation (b) dynamic excitation.

moving speed, however the ballasted track yields marginally higher deviatoric stresses than the slab track. The lower stresses in the slab track are mainly due to the HBL which is stiffer compared to the ballast and sub-ballast. Considering the dynamic excitation, it is shown in Fig. 20(b), Fig. 21(b) and Fig. 22(b) that an increase in moving speed induces significantly higher deviatoric stresses, particularly within the ballasted track. Unlike the quasi-static excitation, the deviatoric stresses

due to the dynamic excitation slightly decrease with depth in all the track layers, particularly at lower speed. These increases in both quasi-static and dynamic deviatoric stresses with speed contribute towards larger permanent deformation and thus differential settlement.

Fig. 23(a) and (b) show the cumulative permanent strains over 90MGT traffic for both ballasted track and slab tracks. These responses are calculated using the mean deviatoric stresses measured on the top of

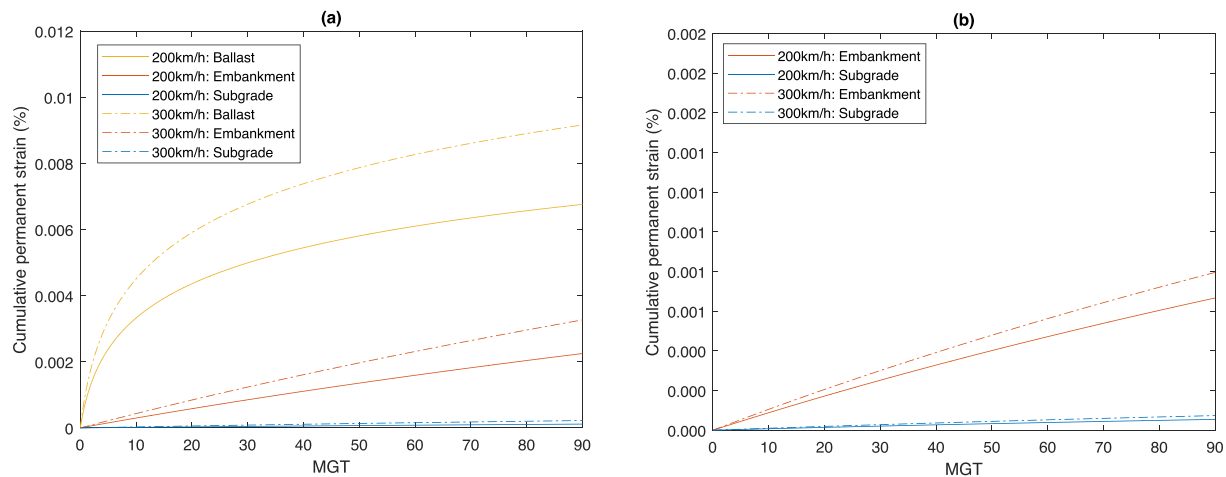


Fig. 23. Cumulative permanent strains: (a) ballasted track (b) slab track.

each layer. However, the iterative process updates the track geometry profile from the settlements calculated every 0.2 m along track length (in the train passage direction) and at vertical depth intervals of 0.25 m. Comparing the cumulative permanent strains in the track and subgrade layers, it is seen that they are lowest in the subgrade layer for both ballasted track and slab track. This is because the settlement primarily occurs in the track-bed layers. For the ballasted track this is because the scope for particle rearrangement is greatest within the ballast matrix. Further, comparing the ballasted track and slab track, the cumulative permanent strains in the ballasted track are higher than the slab track, particularly at high moving speed. This is because the bending stiffness of the slab results in a more uniform distribution of stresses into the supporting earthworks. This is corroborated in Fig. 22(b), where the deviatoric stresses decrease almost linearly with depth below the slab, but non-linearly below the ballasted track. Note that the y-axis in Fig. 23 (b) is scaled $6 \times$ larger than in Fig. 23(a) for improved visibility.

5. Discussion

The numerical results show the rate of geometry degradation is more rapid for ballasted tracks compared to concrete slabs. This is true for speeds of 200 and 300 km/h, however the ballasted track shows more rapid degradation at higher speed. This is because the elevated stress fields propagating within the unbound ballast trackbed can induce significant particle rearrangement. In contrast, the stress fields propagating in the slab track induce negligible plastic deformation within the concrete. Therefore ballasted track permanent settlement is a combination of ballast embankment and subgrade deformation, whereas the concrete slab track settlement is due to the embankment and subgrade deformation. Note however that this study is focused on differential settlements induced solely due to train loading and ignores other sources of long-term earthwork settlements (e.g. consolidation, creep and shrink-swelling). Slab track rail fasteners can be adjusted typically between +26 mm and -4mm to restore track geometry. However, this range relates to the total settlement, meaning the train loading induced differential and uniform settlement must also be considered in conjunction with all additional sources of settlement (e.g. earthworks related settlement).

Further, in reality a range of concrete slab track products exist, including precast and those poured in-situ. The 2.5D modelling procedure used in this paper assumes the concrete slab track is infinitely long and is in absence of expansion joints. Therefore it doesn't account for the additional plastic settlement induced by movements in the vicinity of these joints. Thus, the results are more representative of slab track systems with larger spacing between joints. To study the effect of such discontinuities a 3D model should be considered.

To allow a fair comparison, the analysis has assumed that the track structure and track geometry is the same for both slab and concrete tracks regardless of linespeed. In reality however, ballasted tracks have less onerous earthworks requirements meaning their formation may be less stiff compared to a slab track constructed at the same site. Similar is true when comparing the lower and higher speed track scenarios. Regarding track geometry, at higher speeds the ballasted track geometry is likely to be maintained to a tighter tolerance compared to the low speed. Further, concrete slab tracks are likely to exhibit a lower standard deviation in track geometry post-construction due to higher precision construction methods.

6. Conclusions

Slab track systems are typically considered to be cost-effective if the initial cost is less than 30% greater than ballasted track. Although slab tracks typically require the construction of more highly engineered earthworks, ballasted tracks can be more expensive to maintain due to the need for regular tamping to maintain track geometry within threshold tolerance. To compare the train-induced settlement behaviour of both ballasted and slab tracks, a numerical model was developed capable of simulating track geometry degradation due to repeated train passages. The model is validated for both ballast and concrete slab tracks and then used to study the differential settlement of both track structures at two train speeds: intercity (200 km/h) and high speed (300 km/h). The following conclusions are drawn:

1. Considering the ballasted track, the majority of settlement arises from the ballast layer, due to the rearrangement of particles, rather than the earthworks;
2. Considering the slab track, it's elevated bending stiffness results in a more uniform distribution of stress on the earthworks, resulting lower train-induced strains in the earthwork compared to the ballasted track;
3. Ballasted track exhibits higher differential settlement compared to the slab;
4. At higher linespeeds the degradation of track geometry is more pronounced for the ballasted track compared to slab. This increases further with additional axle passages.

CRediT authorship contribution statement

C. Charoenwong: Methodology, Software, Formal analysis, Validation, Writing – original draft, Writing – review & editing. **D.P. Connolly:** Conceptualization, Methodology, Resources, Supervision, Writing – original draft, Writing – review & editing. **A. Colaço:**

Supervision, Writing – original draft. **P. Alves Costa**: Conceptualization, Supervision. **P.K. Woodward**: Supervision. **A. Romero**: Supervision. **P. Galvín**: Supervision.

Declaration of Competing Interest

The authors declare that they have no known competing financial interests or personal relationships that could have appeared to influence the work reported in this paper.

Data availability

Data will be made available on request.

Acknowledgements

The authors are grateful to the University of Leeds, Leverhulme Trust (PLP-2016-270), the Thai Government and the Spanish Ministry of Science and Innovation and Universities (PID2019-109622RB-C21).

References

- [1] T. Abadi, L. Le Pen, A. Zervos, W. Powrie, A Review and Evaluation of Ballast Settlement Models using Results from the Southampton Railway Testing Facility (SRTF), *Procedia Eng.* 143 (2016) 999–1006.
- [2] P. Alves Costa, R. Calçada, A. Silva Cardoso, Track-ground vibrations induced by railway traffic: In-situ measurements and validation of a 2.5D FEM-BEM model, *Soil Dyn. Earthq. Eng.* 32 (1) (2012) 111–128.
- [3] P. Alves Costa, R. Calçada, A. Silva Cardoso, A. Bodare, Influence of soil non-linearity on the dynamic response of high-speed railway tracks, *Soil Dyn. Earthq. Eng.* 30 (4) (2010) 221–235.
- [4] P. Alves Costa, P. Lopes, A. Silva Cardoso, Soil shakedown analysis of slab railway tracks: Numerical approach and parametric study, *Transp. Geotech.* 16 (2018) 85–96.
- [5] K. Ando, M. Sunaga, H. Aoki, O. Haga, Development of slab tracks for Hokuriku Shinkansen line, *Q. Rep. RTRI (Railw. Tech. Res. Inst.)* 42 (1) (2001) 35–41.
- [6] L. Auersch, S. Said, Track-soil dynamics – Calculation and measurement of damaged and repaired slab tracks, *Transp. Geotech.* 12 (2017) 1–14.
- [7] Auersch, L., Said, S., 2019. Measurement of slab track behaviour at different sites. In: *Proceedings of the 26th International Congress on Sound and Vibration, ICSV 2019*, pp. 1–8.
- [8] R. Bastin, Development of German non-ballasted track forms, *Proc. Inst. Civ. Eng. Transp.* 159 (1) (2006) 25–39.
- [9] C. Charoenwong, D.P. Connolly, K. Odolinski, P. Alves Costa, P. Galvín, A. Smith, The effect of rolling stock characteristics on differential railway track settlement: An engineering-economic model, *Transp. Geotech.* 37 (2022) 100845.
- [10] C. Charoenwong, D.P. Connolly, P.K. Woodward, P. Galvín, P. Alves Costa, Analytical forecasting of long-term railway track settlement, *Comput. Geotech.* 143 (2022) 104601.
- [11] C. Chen, G.R. McDowell, An investigation of the dynamic behaviour of track transition zones using discrete element modelling, *Proc. Inst. Mech. Eng. Part F J. Rail Rapid Transit* 230 (1) (2016) 117–128.
- [12] P. Chumyen, D.P. Connolly, P.K. Woodward, V. Markine, The effect of soil improvement and auxiliary rails at railway track transition zones, *Soil Dyn. Earthq. Eng.* 155 (2022) 107200.
- [13] A. Colaço, P.A. Costa, D.P. Connolly, The influence of train properties on railway ground vibrations, *Struct. Infrastruct. Eng.* 12 (5) (2016) 517–534.
- [14] D.P. Connolly, P.A. Costa, Geodynamics of very high speed transport systems, *Soil Dyn. Earthq. Eng.* 130 (2020) 105982.
- [15] D.P. Connolly, K. Dong, P. Alves Costa, P. Soares, P.K. Woodward, High speed railway ground dynamics: a multi-model analysis, *Int. J. Rail Transp.* 8 (4) (2020) 324–346.
- [16] P.A. Costa, R. Calçada, A.S. Cardoso, Influence of train dynamic modelling strategy on the prediction of track-ground vibrations induced by railway traffic, *Proc. Inst. Mech. Eng. Part F J. Rail Rapid Transit* 226 (4) (2012) 434–450.
- [17] T. Dahlberg, Some railroad settlement models - A critical review, *Proc. Inst. Mech. Eng. Part F J. Rail Rapid Transit* 215 (4) (2001) 289–300.
- [18] A. de Miguel, A. Lau, I. Santos, Numerical simulation of track settlements based on an iterative holistic approach, *J. Brazilian Soc. Mech. Sci. Eng.* (2018) 40.
- [19] A.F. Esen, P.K. Woodward, O. Laghrouche, T.M. Čebašek, A.J. Brennan, S. Robinson, D.P. Connolly, Full-scale laboratory testing of a geosynthetically reinforced soil railway structure, *Transp. Geotech.* 28 (2021) 100526.
- [20] Federal Railroad Administration, 1980. *Statistical Representations of Track Geometry : Volume I*. Washington, D.C.
- [21] R.D. Fröhling, Prediction of Spatially Varying Track Settlement, in: *Conference On Railway Engineering CORE98*, 1998, pp. 103–109.
- [22] P. Galvín, A. Romero, J. Domínguez, Vibrations induced by HST passage on ballast and non-ballast tracks, *Soil Dyn. Earthq. Eng.* 30 (9) (2010) 862–873.
- [23] I. Grossoni, W. Powrie, A. Zervos, Y. Bezin, L. Le Pen, Modelling railway ballasted track settlement in vehicle-track interaction analysis, *Transp. Geotech.* 26 (2021) 100433.
- [24] Y. Guo, W. Zhai, Long-term prediction of track geometry degradation in high-speed vehicle–ballastless track system due to differential subgrade settlement, *Soil Dyn. Earthq. Eng.* 113 (2018) 1–11.
- [25] Y. Guo, C. Zhao, V. Markine, G. Jing, W. Zhai, Calibration for discrete element modelling of railway ballast: A review, *Transp. Geotech.* 23 (2020) 100341.
- [26] B. Indraratna, S. Nimbalkar, Stress-Strain Degradation Response of Railway Ballast Stabilized with Geosynthetics, *J. Geotech. Geoenviron. Eng.* 139 (5) (2013) 684–700.
- [27] B. Indraratna, P.K. Thakur, J.S. Vinod, W. Salim, Semiempirical Cyclic Densification Model for Ballast Incorporating Particle Breakage, *Int. J. Geomech.* 12 (3) (2012) 260–271.
- [28] A. Karlström, A. Boström, An analytical model for train-induced ground vibrations from railways, *J. Sound Vib.* 292 (1-2) (2006) 221–241.
- [29] G. Kouroussis, D.P. Connolly, O. Verlinden, Railway-induced ground vibrations – a review of vehicle effects, *Int. J. Rail Transp.* 2 (2) (2014) 69–110.
- [30] N. Kumar, C. Kossmann, S. Scheriau, K. Six, An efficient physical-based method for predicting the long-term evolution of vertical railway track geometries, *Proc. Inst. Mech. Eng., Part F: J. Rail Rapid Transit* 236 (4) (2022) 447–465.
- [31] A.C. Lamprea-Pineda, D.P. Connolly, M.F.M. Hussein, Beams on elastic foundations – A review of railway applications and solutions, *Transp. Geotech.* 33 (2022), 100696.
- [32] D. Li, E.T. Selig, Resilient modulus for fine-grained subgrade soils, *J. Geotech. Eng.* 120 (1994) 939–957.
- [33] D. Li, E.T. Selig, Cumulative Plastic Deformation for Fine-Grained Subgrade Soils, *J. Geotech. Eng.* 122 (1996) 1006–1013.
- [34] J. Liu, J. Xiao, Experimental Study on the Stability of Railroad Silt Subgrade with Increasing Train Speed, *J. Geotech. Geoenviron. Eng.* 136 (2010) 833–841.
- [35] T. Marolt Čebašek, A.F. Esen, P.K. Woodward, O. Laghrouche, D.P. Connolly, Full scale laboratory testing of ballast and concrete slab tracks under phased cyclic loading, *Transp. Geotech.* 17 (2018) 33–40.
- [36] M. Menan Hasnayn, W. John McCarter, P.K. Woodward, D.P. Connolly, G. Starrs, Railway subgrade performance during flooding and the post-flooding (recovery) period, *Transp. Geotech.* 11 (2017) 57–68.
- [37] S. Miura, H. Takai, M. Uchida, Y. Fukada, The Mechanism of Railway Tracks, *Japan Railw. Transp. Rev.* 3 (1998) 38–45.
- [38] J.C.O. Nielsen, X. Li, Railway track geometry degradation due to differential settlement of ballast/subgrade – Numerical prediction by an iterative procedure, *J. Sound Vib.* 412 (2018) 441–456.
- [39] ORE, Question D71: Stresses in the Rails, the Ballast and in the Formation Resulting from Traffic Loads. Stresses in the formation (results of the third phase; measurements under dynamic conditions), International Union of Railways, Office for Research and Experiments, 1970.
- [40] A. Ramos, A. Gomes Correia, R. Calçada, P. Alves Costa, Stress and permanent deformation amplification factors in subgrade induced by dynamic mechanisms in track structures, *Int. J. Rail Transp.* 00 (2021) 1–33.
- [41] A. Ramos, A. Gomes Correia, R. Calçada, P. Alves Costa, A. Esen, P.K. Woodward, D.P. Connolly, O. Laghrouche, Influence of track foundation on the performance of ballast and concrete slab tracks under cyclic loading: Physical modelling and numerical model calibration, *Constr. Build. Mater.* 277 (2021), 122245.
- [42] A. Ramos, A. Gomes Correia, B. Indraratna, T. Ngo, R. Calçada, P.A. Costa, Mechanistic-empirical permanent deformation models: Laboratory testing, modelling and ranking, *Transp. Geotech.* (2020) 23.
- [43] Y. Sato, Japanese Studies on Deterioration of Ballasted Track, *Veh. Syst. Dyn.* 24 (1995) 197–208.
- [44] G. Saussine, C. Cholet, P.E. Gautier, F. Dubois, C. Bohatier, J.J. Moreau, Modelling ballast behaviour under dynamic loading. Part 1: A 2D polygonal discrete element method approach, *Comput. Methods Appl. Mech. Eng.* 195 (2006) 2841–2859.
- [45] M.A. Sayeed, M.A. Shahin, Design of ballasted railway track foundations using numerical modelling. Part I: Development I, *Can. Geotech. J.* 55 (2018) 353–368.
- [46] Y. Shan, S. Zhou, H. Zhou, B. Wang, Z. Zhao, Y. Shu, Z. Yu, Iterative method for predicting uneven settlement caused by high-speed train loads in transition-zone subgrade, *Transp. Res. Rec.* 2607 (2017) 7–14.
- [47] M.J. Shenton, Ballast deformation and track deterioration, *Track Technol.* (1985) 253–265.
- [48] J. Shi, A.H. Chan, M.P.N. Burrow, Influence of unsupported sleepers on dynamic responses of railroad embankment below a heavy haul railway line using simulation techniques, *RRUKA Annu. Conf.* (2012) 1–6.
- [49] S. Shi, L. Gao, B. Hou, M. Xu, Y. Xiao, Numerical investigation on multiscale mechanical properties of ballast bed in dynamic stabilization maintenance, *Comput. Geotech.* 144 (2022), 104649.
- [50] J.Y. Shih, I. Grossoni, Y. Bezin, Settlement analysis using a generic ballasted track simulation package, *Transp. Geotech.* 20 (2019), 100249.
- [51] A.S.J. Suiker, R. de Borst, A numerical model for the cyclic deterioration of railway tracks, *Int. J. Numer. Meth. Eng.* 57 (2003) 441–470.
- [52] S.D. Tayabji, D. Bilow, Concrete slab track state of the practice, *Transp. Res. Rec.* (2001) 87–96.
- [53] D. Whitehead, T. Lead, M. Rippin, H. Road, O.E. Street, Level 2 Standard Track Geometry, Gauging and Clearances (2021) 1–68.
- [54] Z. Yu, P.K. Woodward, O. Laghrouche, D.P. Connolly, True triaxial testing of geogrid for high speed railways, *Transp. Geotech.* 20 (2019), 100247.
- [55] W. Zhai, Z. Cai, Dynamic interaction between a lumped mass vehicle and a discretely supported continuous rail track, *Comput. Struct.* 63 (1997) 987–997.